CARBON 47 (2009) 2174–2185

available at www.sciencedirect.com

ScienceDirect

journal homepage: www.elsevier.com/locate/carbon

Analytical investigation of the composition of plasma-induced functional groups on carbon nanotube sheets

Nicolas Peer Zschoerper[a,b,*], *Verena Katzenmaier*[a,b], *Uwe Vohrer*[a], *Michael Haupt*[a], *Christian Oehr*[a], *Thomas Hirth*[a,b]

[a]*Fraunhofer Institute for Interfacial Engineering and Biotechnology, Nobelstrasse 12, 70569 Stuttgart, Germany*
[b]*Institute for Interfacial Engineering, University of Stuttgart, Nobelstrasse 12, 70569 Stuttgart, Germany*

ARTICLE INFO

Article history:
Received 16 February 2009
Accepted 27 March 2009
Available online 5 April 2009

ABSTRACT

To increase the applicability of carbon nanotubes (CNTs) oxygen-containing functional groups were generated on their widely inert surface by using glow-discharge plasmas. CNT-sheets (bucky papers) produced from the powder-like raw material were used as substrates allowing for a more defined characterization of one and the same surface by different analytical techniques. The plasma composition was analyzed by optical emission spectroscopy. Since the actual composition of the plasma-induced functional groups has still not been completely resolved, we performed an in-depth characterization of the treated samples by X-ray photoelectron (XPS) and Raman spectroscopy as well as electron spin resonance measurements. To overcome limitations of the XPS-analysis in distinguishing between groups featuring nearby binding energies, alcohol-, keto-/aldehyde-, and carboxyl-groups were tagged by derivatization techniques using fluorine-containing reagents (trifluoroaceticanhydride, trifluoromethylphenylhydrazine, and trifluoroethanol). Differential spectra were calculated to enhance the accuracy of the deconvolution of the XPS-spectra. This enabled us to determine dependencies of the plasma parameters, i.e. treatment time, process pressure, and gas composition (mixtures of Ar, O_2, H_2O, and H_2), on the composition of the generated functional groups as well as an up to 6-fold enhancement in derivatizable groups for switching process gas from Ar/O_2 to Ar/H_2O.

1. Introduction

Although multi walled carbon nanotubes (MWCNTs) have already been reported on in 1952 [1], it was not until Iijima's findings in 1991 [2] that MWCNTs re-entered the focus of numerous researchers of academia and industry. With the discovery of single walled carbon nanotubes (SWCNTs) by Iijima and Ichihashi [3] and Bethune et al. [4], the scientific community was given a more ideal material to explore the outstanding physical and chemical properties proposed for carbon nanotubes (CNTs) as well as their exploitation in applications [5–7]. Despite of improvements in the production of both MWCNTs and SWCNTs a purification of the as-produced material is usually imperative. Unless residual metallic catalyst is covered by the end-cap of the CNT, it can be removed by HCl or other strong acids such as H_2SO_4 or HNO_3 as well as combinations of those and other oxidizing agents. While the first treatment should not affect the CNT itself, the latter kinds also introduce oxygen functionalities to the CNTs and are often carried out for their use in further wet chemical functionalizations. For the CNTs being widely chemically inert and inherently hydrophobic, such function-

* *Corresponding author:* Address: Fraunhofer Institute for Interfacial Engineering and Biotechnology, Nobelstrasse 12, 70569 Stuttgart, Germany. Fax: +49 711 970 4200.
E-mail address: nicolas.zschoerper@igb.fraunhofer.de (N.P. Zschoerper).
0008-6223/$ - see front matter
doi:10.1016/j.carbon.2009.03.059

alizations are considered to be required for most intended applications, yet the rather harsh conditions needed for wet chemical functionalization of CNTs [8–11] have raised a demand for alternative methods.

Since the 1960s plasma technology has quickly evolved into a valuable technique to engineer surface properties without alteration of the bulk composition [12,13] and is nowadays used in various applications such as plasma cleaning, plasma sterilization, plasma coatings, fluorination, and biomedical applications [14]. We have therefore utilized low pressure glow-discharge plasmas to modify CNTs [15] in a facile and environmentally sound manner, avoiding the discerning conditions as well as a comparatively high consumption and accompanying wastage of chemicals wet chemical methods require.

For this technique, different types of experimental or commercial reactor designs have been described, e.g. custom-built fluidized bed reactors providing a scalable way of modifying particulate systems, i.e. the powdery raw material itself, in a homogeneous manner [16,17] or regular and modified parallel plate reactors [18,19] predominantly used to treat CNT sheets, so-called bucky papers. While plasma treatment can modify the substrate surface in terms of coating, functionalization, and/or etching, especially plasma functionalization, i.e. generation of surface-bound functional groups without deposition of a coating, is considered a promising solution to enhance the reactivity of CNTs. Tseng et al. as well as Yan et al. functionalized CNTs by plasma activation in argon plasma followed by grafting of maleic anhydride [20] or 1-vinylimidazole [21,22]. However, the use of other process gases enables direct generation of functional groups. Process gases like N_2, Ar/N_2, or NH_3 were used to generate amine- and nitrile-groups [23–26]. Due to their polar character and sufficient stability, especially oxygen-containing groups are aspired as well. While the effect of oxygen or oxygen-containing plasmas on CNTs could already be shown e.g. in terms of tuning of the wettability up to spontaneous wetting [19,27,28] or improved adhesion of metal nanoparticles [29,30], the identification of the functional groups generated thereby and thus their (semi)quantitative evaluation has still not been resolved. Characterization of the modified samples by FT-IR proved existence of C–OH, C=O, and COOH functionalities after oxygen or water plasmas [31–35], yet neither FT-IR nor XPS analysis could completely resolve the difficulties with regard to quantification of such groups. Since little is known about proper fitting of XPS spectra of functionalized CNT samples, experience from corresponding procedures for polymer substrates cannot be easily transferred. Thus, analysis so far was limited to comparison of the overall elemental composition, especially the oxygen content [16,23,36,37], as well as general statements upon the existence of the different oxygen-containing functional groups based on changes seen in the C1s spectrum [16,23,36]. Additionally, since signals from alcohol- and ether-groups as well as carboxyl- and ester groups overlay in the C1s spectrum, analysis of the spectrum does not provide information about the distribution of those groups. Hence, we have performed derivatization reactions after exposing samples cut from bucky papers to plasmas using process gases like Ar/O_2, $Ar/O_2/H_2$, $Ar–H_2O/O_2$, or $Ar–H_2O$ in order to enhance accessibility of specific functional groups on the surface to XPS analysis. We have furthermore used differential spectra to account for the asymmetric tail pristine, i.e. unmodified, CNTs feature in their C1s spectrum usually complicating application of a fitting routine. ESR measurements were conducted for assessment of dangling bonds or degree of saturation of such, respectively. For additional information on the plasma-induced functional groups, Raman spectra were recorded before and after plasma modification and analyzed with respect to D-band shifts and the D/G^- area ratios.

2. Materials and methods

2.1. Bucky paper production

In the style of a purification procedure for SWCNT raw material described by Rinzler et al. [38], HCl-purified MWCNT material provided by FutureCarbon GmbH ("CNT-MW, purified") was dispersed at a concentration of 1 mg/ml in a 0.01 M aqueous solution of sodium dodecylsulphate (SDS) purchased from Carl Roth GmbH (purity $\geqslant$ 99%) using ultrasonication for 30 min. The dispersion was subsequently centrifuged at 4500 RCF. For each bucky paper, 150 ml of the supernatant was pressure-filtered at 5 bar employing a polycarbonate filter membrane (0.4 μm pore size, obtained from Carl Roth GmbH) and washed with deionized water (55 °C) to remove residual SDS. The bucky paper, i.e. the black filter cake (diameter ~78 mm, thickness 30–40 μm), was peeled off from the filter membrane after drying and cut into adequate samples for analysis by XPS, Raman, and ESR.

2.2. Plasma modification

Bucky paper samples were treated in a parallel plate reactor consisting of two aluminum electrodes with a size of 450 mm × 350 mm, separated by a polycarbonate frame with a height of about 40 mm. The plasma was capacitively coupled at a frequency of 13.56 MHz (radio frequency, RF). The upper electrode was connected to the RF, while the lower one was grounded.

The plasma treatments were carried out using argon, hydrogen (both 5.0 grade), and oxygen (4.5 grade). Unless noted differently, the argon flow was 45.1 sccm, whereas the flows for oxygen or hydrogen were set to 0.9 sccm. For the $Ar–H_2O$-plasma treatments, argon was bubbled through deionized water at a primary pressure of 0.5 bar and a flow of 16 sccm for a process pressure of 120 μbar and a flow of 48 sccm for all other process pressures. The pressure was controlled and set via a type 651C digital PID pressure controller connected to both, a type 626A Baratron® absolute capacitance manometer and a type 653B throttle valve (all obtained from MKS Instruments Deutschland GmbH).

All treatments were performed at a load of 20 W, whereas pressure and treatment time were varied.

2.3. Derivatization

After plasma treatment, three different derivatization reactions were performed using fluorine-containing agents in a

custom-built derivatization reactor. Due to the higher selectivity, all reactions were carried out in a saturated vapor phase. Therefore derivatization agents were measured into an argon-filled reservoir and frozen using a liquid nitrogen (LN_2)-dewar before evacuating reactor and reservoir until a pressure $\leqslant 1 \times 10^{-2}$ mbar was reached. The dewar was then removed to promote the derivatization agent into the vapor phase upon unfreezing. Samples were left under this condition over night before the reservoir was removed and the reactor was evacuated again for at least 5 h to remove physisorbed reagent. To account for irremovable physisorbed reagent and/or unspecific binding, respective unmodified samples were derivatized in the same manner and differences in the fluorine contents were calculated after respective XPS analysis.

Following the literature [39,40], 400 μl of trifluoroaceticanhydride (TFAA) were used for a total reactor-volume of about 200 ml to derivatize alcohol groups. For derivatization of keto- and aldehyde-groups, Briggs and co-workers [41,42] described a method using the ability of those groups to convert hydrazine to hydrazone in a Wolff–Kishner-reaction [39,43] followed by quantification of nitrogen using XPS. In order to profit from the higher sensitivity factor of fluorine, we employed trifluoromethylphenylhydrazine (TFMPH) instead. In this case approximately 200 mg were weighed in. While room temperature and the decreased base pressure are sufficient for the necessary phase change in case of the other reagents, TFMPH furthermore needed to be heated to ~80 °C to attain vapor phase. To derivatize carboxyl groups, a combination of 56 μl trifluoroethanol (TFE), 25 μl pyridine, and 20 μl di-*tert*-butylcarbodiimide was used on the basis of the procedure described by Sabbatini and Zambonin [39].

2.4. *Instrumentation and analysis*

Optical emission spectroscopy (OES) was conducted using a SpectraPro®-275 (Acton Research Corporation) spectrograph. Spectra were recorded from 190 nm to 900 nm at 20 μm slot width, 500 ms exposure time, 10 accumulations, and a 1200 lines/mm-grating, keeping pressure constant and combined gas flow at about 46 sccm. Spectra were analyzed by Plasus SpecLine software taking into account a spectral resolution of ±0.3 nm.

Samples were analyzed by XPS employing a Kratos Axis Ultra System equipped with a DLD-detector and a monochromatic Al Kα X-ray source. Further details of the setup can be found in [44,45]. Spectra were analyzed by CasaXPS 2.3.14 software. Spectra were calibrated setting the aliphatic carbon to 284.6 eV. For detailed analysis of the C1s spectrum, the components and restrictions summarized in Table 1 were employed (also see Fig. 3). Full width at half maximum (FWHM) was allowed to adjust freely for $C_{aliphatic}$ and usually attained values around 0.8 eV, while FWHM were restricted to 0.80–1.45 eV for all other components except for $C_{shakeup2}$ and $C_{shakeup3}$ for which restrictions were set to 0.8–2.0 eV. Since in case of a direct functionalization changes in the C1s spectra upon plasma modification are basically due to rearrangements of the atomic bonds, C1s spectra were area-normalized and differential spectra were generated subtracting the spectrum of a non-treated sample.

Table 1 – C1s component assignment and applied restrictions (binding energy ranges) of the XPS-fitting routine.

Component (see Fig. 3)	(1)	(2)	(3a)	(3b)	(4a)	(4b)	(5a)	(5b)	(6)	(7)	(8)
Assignment	$C_{aliphatic}$	C2	C–O–C and C_{epoxy}	C–OH	$C{=}O_{non\text{-}derivatizable}$	C=O	COOC	COOH	$C_{shakeup1}$	$C_{shakeup2}$	$C_{shakeup3}$
Binding energy (eV)	283.0–285.0	285.0–286.0	286.1–286.8		286.4–288.1		288.6–289.4		289.5–291.5	291.5–293.5	293.5–295.0

ESR measurements were conducted at room temperature on a Magnettech MS200 high sensitivity system at 16 mW input power and 3.5 G field modulation with a sweep of 1 G/s. Transfer time between plasma-off and ESR measurement was kept constant at 8 min ensuring comparability of the determined values since the recombination of dangling bonds is time dependant.

Raman spectra were collected using an Ntegra Spectra system (NT-MDT) coupled to an Olympus microscope. A 100× (NA = 0.95) objective was used to focus the laser on the sample. Lateral spot size was ~400 nm and focus depth was ~700 nm. The samples were excited with a 633 nm (He–Ne) laser with an incident power on the samples of ~3 mW/μm^2. The 1200 lines/mm-grating of the spectrometer and the 50 μm pinhole of the monochromator resulted in a spectral resolution of 1.2 cm^{-1} to resolve Raman line shifts.

3. Results and discussion

For the experiments conducted using Ar/O_2-plasmas the process gas mixture was optimized using OES in order to obtain a high content of atomic oxygen to benefit from its high reactivity. In the following we investigated the pressure and time dependency of plasmas on the distribution of the (derivatizable) functional groups at that determined composition. Finally, those results were compared to those obtained from Ar–H_2O-plasmas at various pressures as well as to those obtained from intermediate process gas mixtures, i.e. Ar/O_2/H_2 and Ar–H_2O/O_2.

3.1. *Generation of plasmas with high atomic oxygen content*

Performing a plasma functionalization, surface functional groups are generated more or less under retention of the original surface and without deposition of an actual coating. Judging from previous studies on oxygen-containing plasmas on SWCNT bucky papers [15], a maximum total oxygen content of about 30 atom% can be assumed for CNT-modification.

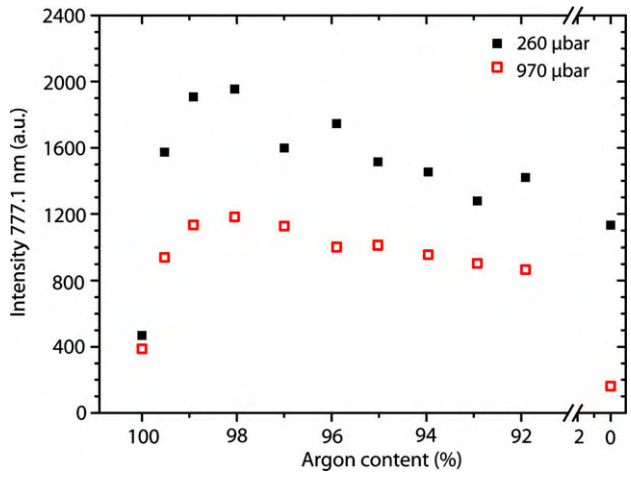

Fig. 1 – Emission intensities at 777.1 nm measured for Ar/O_2-plasmas at 260 μbar (solid squares) and 970 μbar (open squares).

This means that the surface of a bucky paper is, also after plasma functionalization, primarily comprised of carbon. Thus, the probability of an activated molecule or atom colliding with a pristine, i.e. unmodified, non-oxidized carbon atom is much higher than its reaction with a surface functionality generated beforehand. A plasma composition with a high yield of atomic oxygen should therefore result in an increased amount of oxygen functionalities comprising a single oxygen. In order to provide for such a plasma composition, we optimized the process gas mixture (Ar/O_2) for a maximum content of optical emitting species of atomic oxygen. OES-spectra were therefore acquired for Ar/O_2-plasmas, varying the argon content from 100% to 90%. The lines measured at 777.1 nm and 844.5 nm are both within the margin of error to be assigned to atomic oxygen. Although being comparatively insignificant lines, signals could be detected at those

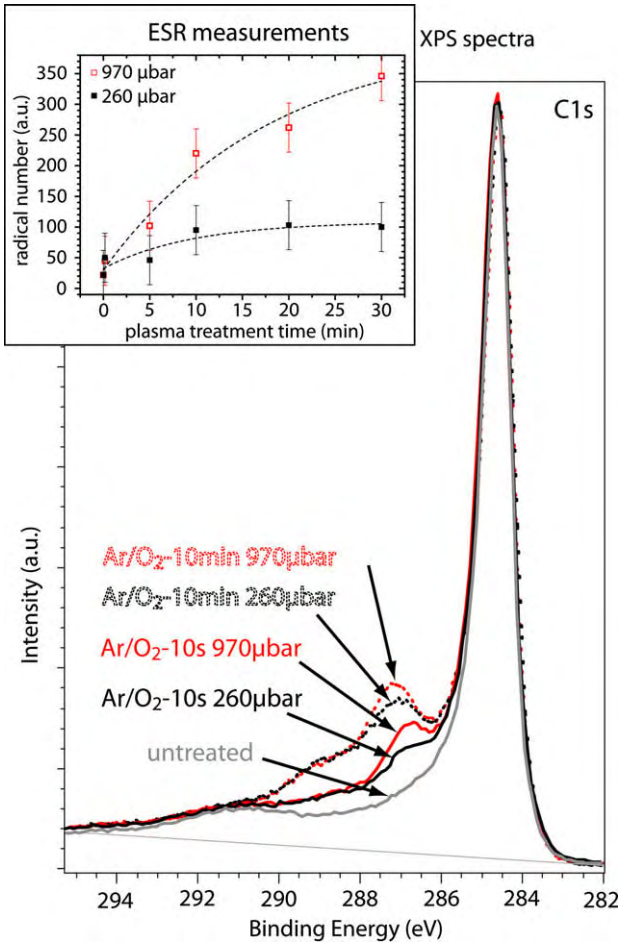

Fig. 2 – XPS-C1s-spectra of an untreated bucky paper and after 10 s and 10 min treatment in an Ar/O_2-plasma at 260 μbar and at 970 μbar exhibiting an increase at ~287 eV with increasing pressure as well as generally higher photoelectron intensities at binding energies >286 eV for the 10 min treatments indicating more extensive functionalization. Inset is depicting ESR measurements featuring the radical number in dependency of the treatment time for 260 μbar (solid squares) and 970 μbar (open squares).

wavelengths in the spectra obtained from pure argon plasmas as well. This is due to the existence of argon emission lines at 776.8 nm and 844.6 nm which thus are, in our setup, indistinguishable from the oxygen lines mentioned above. It is therefore to be assumed that the respective argon emission contributes to the intensity measured for Ar/O_2-plasmas. Despite those difficulties a considerable increase in intensity of emission at both wavelengths was found for both 260 μbar and 970 μbar process pressure compared to the intensities measured for a pure argon or pure oxygen plasma. Since, according to those measurements, the contribution of the argon emission to the 844.5 nm intensity is considerably large, we evaluated the 777.1 nm line where the contribution of the argon emission is negligible compared to the measured increase in intensity due to the oxygen added (see Fig. 1). This line featured a maximum intensity at a composition of 98% argon and 2% oxygen for both pressures and was therefore chosen for the subsequent experiments. Additional measurements using MW-interferometry on the plasmas furthermore held a higher electron density of $3.75 \pm 0.55 \times 10^8$ electrons/cm^3 for 260 μbar compared to $2.75 \pm 0.15 \times 10^8$ electrons/cm^3 for 970 μbar agreeing with the absolute intensities at 777.1 nm and 844.5 nm seen via OES, which were also lower for 970 μbar, and militating for a lower number of the respec-

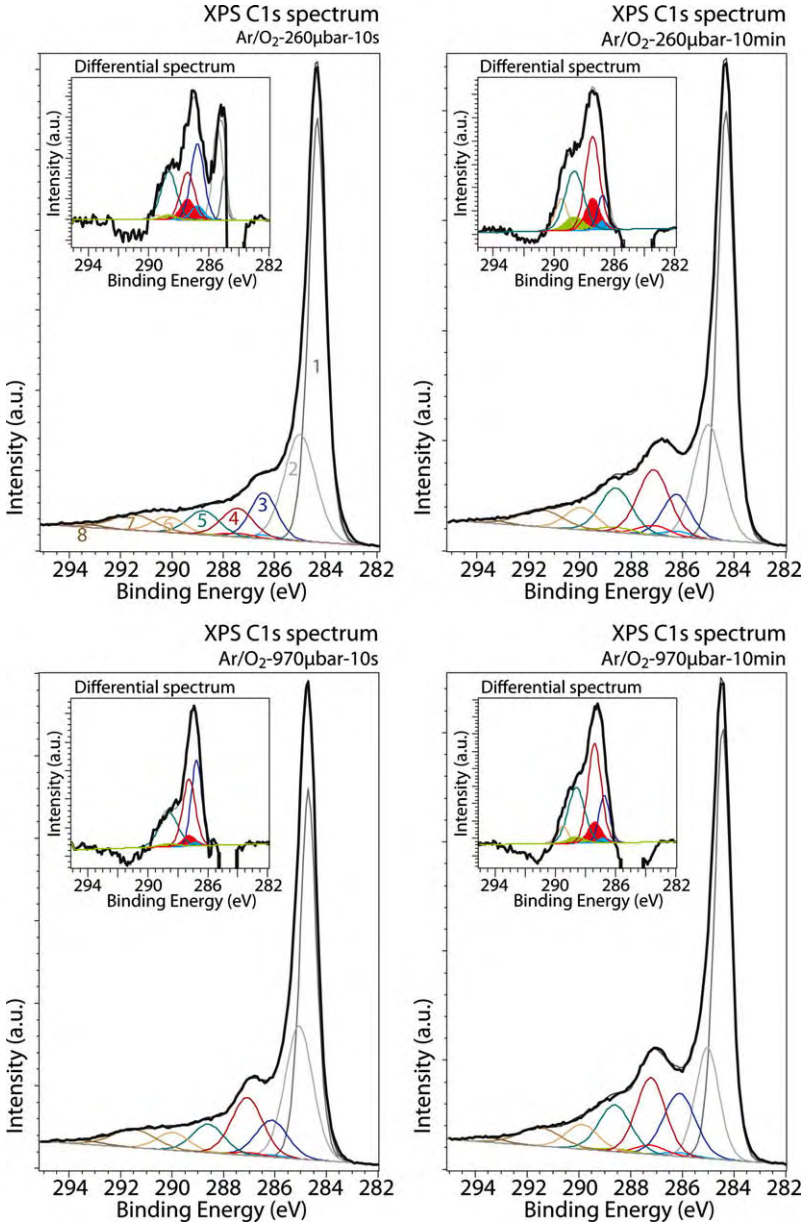

Fig. 3 – XPS spectra of samples Ar/O_2-plasma-treated at 20 W and 260 μbar (top row) or 970 μbar (bottom row) for 10 s (left column) or 10 min (right column) including fitted components 1–8. Insets show corresponding differential spectra with derivatizable contents of alcohol (dark grey/light blue area), keto-/aldehyde (black/light red area), and carboxyl-groups (light grey/light green area). (For interpretation of the references to color in this figure legend, the reader is referred to the web version of this article.)

tive activated species due to reduced power per particle at the higher pressure.

3.2. Pressure dependency of Ar/O_2-plasmas

Bucky paper samples were treated in Ar/O_2-plasmas for 10 s or 10 min at 260 μbar and 970 μbar employing the above mentioned gas composition and were subsequently analyzed by XPS. As is to be expected, the longer treatment time of 10 min also results in considerably higher photoelectron intensities throughout the entire asymmetric tail in the C1s spectrum at higher binding energies, denoting a higher degree of functionalization. While the C1s spectrum of an untreated sample also holds an asymmetric tail akin to graphite [16,23] and shake-up peaks for binding energies >289.5 eV commonly assigned to π–π^* transitions [46], the samples treated at the two different pressures, exhibit a remarkable variation in the intensity of the spectrum at higher binding energies (see Fig. 2).

This can be assigned to oxygen functionalities introduced to the CNTs. Moreover, this feature is more distinct for the higher pressure in both, the 10 s and 10 min treatment, and is accompanied by a significantly larger amount of dangling bonds, i.e. surface-bound radicals, ESR measurements revealed for that pressure and various additional treatment times (see inset Fig. 2). This means, that despite OES- and MW-interferometry measurements indicating a lower concentration of optical emitting species of atomic oxygen and a lower electron density for the higher pressure, XPS- and ESR-results hold an opposite trend. However, it is known from literature that in oxygen-containing plasmas the generation of ozone increases significantly with increasing pressure [47–49]. Furthermore, it has been reported that such ozone generation is enhanced by temperatures especially around or below room temperature [49], i.e. by conditions that are perfectly met by the low pressure plasmas applied in our setup. Ozone reacts, even as a non-excited species, with CNTs [50–54] following the Criegee-mechanism [55] known from polyolefins and fullerenes [56] and leading to epoxy- and ester-groups [50,53] on the CNT surface as well as CO_2 and CO, i.e. etching of the substrate [50,52]. Since etching is most likely to play a major role in generation of dangling bonds, the reason for the increased amount of dangling bonds for the 970 μbar treatments is obviously the combined etching capability of atomic oxygen and ozone at that pressure exceeding the one for 260 μbar where etching is predominantly due to atomic oxygen alone.

For a deeper insight in the processes especially at the plasma–CNT interface, a more detailed knowledge about the kind and amount of the different surface functional groups generated is necessary. However, a straightforward deconvolution of the XPS-C1s spectrum only allows for a rough classification of those groups due to the fact that alcohol-, ether-, and epoxy-groups feature similar binding energies, the same way carboxyl- and ester-groups do, resulting in overlaying signals, respectively, which compose the measured spectrum and impede a direct quantitative analysis (see Table 1). In order to gain a better insight in the contribution of the different oxygen-containing functional groups to the changes seen by the different analysis methods, derivatizations were performed for alcohol-, keto-/aldehyde-, and carboxyl-groups followed by XPS analysis with respect to the fluorine introduced. Results of these experiments at both 260 μbar and 970 μbar are shown in Table 2 for different treatment times, respectively. In Fig. 3, the corresponding spectra are shown together with differential spectra (shown in insets) with derivatizable contents marked as the filled components of the deconvolution. The total carbon and oxygen contents were both derived from the treated non-derivatized sample. The fluorine contents were derived from treated samples after derivatization with the respective agent (TFAA, TFMPH, or TFE). Using the carbon and fluorine contents measured by XPS, the actual content of derivatizable functional groups (see Eqs. (1)–(3)) in groups per 100 carbon atoms was calculated, considering the increase in carbon content by introduction of the derivatization agent to the surface

$$[OH] = 100 * [F_{TFAA}]/(3 * [C_{total,TFAA}] - 2 * [F_{TFAA}]) \quad (1)$$

$$[C{=}O] = 100 * [F_{TFMPH}]/(3 * [C_{total,TFMPH}] - 7 * [F_{TFMPH}]) \quad (2)$$

$$[COOH] = 100 * [F_{TFE}]/(3 * [C_{total,TFE}] - 2 * [F_{TFE}]) \quad (3)$$

In consideration of e.g. unspecific adsorption, respective contents, ascertained for untreated, but derivatized samples, were subtracted from the ones determined for the respective plasma treatment calculating the differences which can be ascribed to specific marking of the functional group (see Eqs. (4)–(6))

$$\Delta[OH] = [OH]_{treated} - [OH]_{untreated} \quad (4)$$

$$\Delta[C{=}O] = [C{=}O]_{treated} - [C{=}O]_{untreated} \quad (5)$$

$$\Delta[COOH] = [COOH]_{treated} - [COOH]_{untreated} \quad (6)$$

The evaluated differences are also shown in Table 2. The remaining functional groups are therefore first of all,

Table 2 – Elemental composition of bucky paper samples treated in an Ar/O_2-plasma at 20 W. Total contents were derived from the plasma-treated samples, fluorine contents were obtained separately for the agent indicated as index. Calculated contents of derivatizable functional groups shown as differences with respect to an untreated sample.

Ar/O_2–20 W	Elemental composition (atom%)					Induced functional groups (per 100 C)		
	C_{total}	O_{total}	F_{TFAA}	F_{TFMPH}	F_{TFE}	Δ[OH]	Δ[C=O]	Δ[COOH]
260 μbar to 10 s	89.6	9.0	1.7	2.0	0.6	0.33	0.51	0.13
260 μbar to 10 min	82.8	16.4	2.2	3.9	2.3	0.27	1.39	0.78
970 μbar to 10 s	91.3	8.4	1.1	1.6	0.7	0.10	0.35	0.14
970 μbar to 5 min	84.9	14.1	1.2	5.0	2.4	0.18	1.55	0.79
970 μbar to 10 min	82.8	16.5	1.6	3.3	1.3	0.21	1.17	0.44

non-derivatized alcohol-groups, whose XPS-signal is overlaid by those of epoxy- and ether-groups, second of all, non-derivatized keto-/aldehyde-groups, and third of all, non-derivatized carboxyl-groups, whose XPS-signal is overlaid by that of ester-groups (see Fig. 3).

According to this analysis technique, the 10 s treatments exhibit basically no difference in content of carboxyl groups, yet the lower pressure resulted in an increase in alcohol and keto-/aldehyde-groups. Although not all of the respective functional groups need to be derivatized for reasons of chemical conversion and general accessibility (also see Section 3.5), the samples treated at the lower pressure prove that a higher density of functionalization is in fact accessible. Thus, the more distinct feature at ~287 eV for the respective treatments at the higher pressure has to be assigned to a respectively larger content of epoxy- and/or ether-groups which are not covered by the TFAA derivatization routine. Since an increased ozone content is to be expected at the higher pressure, it is highly probable that the more distinct feature in the C1s spectrum for this treatment is mainly due to ozone-induced epoxy-groups.

Aside from the expectedly larger total oxygen content, analysis of the 10 min treatments confirmed the above described results, showing higher contents of alcohol- and keto-/aldehyde-groups for the 260 μbar treatment and a more distinct feature ~287 eV especially for the 970 μbar treatment which again can primarily be assigned to ozone-induced epoxy-groups. The spectra at both pressures exhibit higher intensities at ~288.6 eV with respect to the ones with the shorter treatment time, which accommodates the increased oxygen content of ~16.5 atom% for both pressures. However, the carboxyl content decreases with increasing pressure. In reverse, this means that the content in ester groups has to be higher for the 970 μbar treatment. This again agrees with an increased ozone content at this pressure and the reaction channels mentioned above.

Although an ascertainment of values for the contents of the remaining functional groups that are not directly covered by our derivatization would be highly desirable, this is not only prevented by different factors influencing the measurable fluorine content (see Section 3.5), but also by the fact that the spectrum of a pristine CNT-sample also exhibits an asymmetric tail versus higher binding energies. This would bias the values obtainable in case of a simple subtraction of the calculated differences in derivatizable contents. Therefore those differences in derivatizable functional groups were reentered into the fitting routine which was then applied to differential spectra generated from the previously area-normalized spectra of a respective treated and untreated spectrum (see insets Fig. 3). As expected, the differential spectra all featured negative intensities at low binding energies, denoting for the relative "loss" in graphitic carbon due to the plasma modification, which in turn results in the relative "gain" at binding energies up to ~290 eV. The negative intensities measured for binding energies >290 eV indicate a certain disruption of the π-character of the CNTs. With the areas for the known, i.e. derivatizable, components kept constant at their respective percentage of the differential C1s peak area, fitting and quantification of the differential spectra was performed. Although the results obtained from this procedure (data not shown) support the previous data indicating increased amounts of epoxy-groups, ethers, and esters for the treatments at higher pressure, the absolute values of the non-derivatizable components still hold some tolerance due to the amount of available components and the range of their restrictions.

3.3. *Time dependency of Ar/O_2-plasmas*

With respect to the influence of the plasma treatment time, experiments were performed at 10 s, 5 min, and 10 min at a pressure of 970 μbar. The results are shown in Table 2. According to the XPS measurements, an initially strong incorporation of oxygen takes place starting at a content of about 1.5 atom% for the untreated sample which increases to 8.4 atom% after only 10 s. Yet, the process subsequently seems to approach a maximum, since the difference in oxygen content between the 5 min and the 10 min sample is comparatively small. There are two ways to explain this. First, the existence of an upper limit for the oxygenation of the CNTs, and second, an antagonistic effect gaining influence with increasing treatment time. In the dynamic process at hand, the first follows the idea that the carbon lattice of the CNT can only be altered to a certain extent. Further addition of oxygen would also lead to a certain loss, i.e. an antagonistic effect, which is easily identified as generation of carbon monoxide or –dioxide that are extracted through the vacuum system. This etching effect is known particularly for oxygen-containing plasmas.

This is also reflected in the contents of derivatizable functional groups: Although the absolute oxygen content increases from ~14 atom% for 5 min to ~16.5 atom% for 10 min treatment time, the 5 min treatment exhibits, in sum, more functional groups accessible and converted by the derivatization agents, while the contents more or less decrease towards the longest treatment time of 10 min (see Table 2). Only the content in alcohol groups attains slightly higher values for the 10 min treatment since those groups are likely to evolve from the reaction of water vapor from the ambient air with dangling bonds upon opening the reactor. However, since the feature at ~287 eV in the C1s spectrum is considerably more distinct for the 10 min treatment than for the 5 min treatment, it cannot be explained by this small difference in alcohol groups alone, but has to be due to larger contents of ether- and especially epoxy-groups. Although the latter are likely to be generated in the higher pressure regime for the above described reasons, the derivatization data does not provide information about the actual content of either of the two. The region around 289 eV holds similar trends. Despite of an increased oxygen content for the 10 min treatment and similar spectra for binding energies >288 eV, the content of carboxyl-groups decreases from Δ[COOH] = 0.79 groups/100 C-atoms for 5 min to Δ[COOH] = 0.44 groups/100 C for 10 min. In reverse, this means that the content in ester groups has to be larger for the longer treatment time.

Since all treatments were carried out at a pressure of 970 μbar, the reason for the determined differences is threefold: Firstly, it is to be expected that the contents of ozone-induced functional groups such as epoxy- and ester-groups increase with increasing treatment time. Secondly, especially

ether- and ester-groups are less reactive, i.e. more stable, and thus more resistant towards an oxidative attack, whereas especially carboxyl-groups attached to the CNT lattice offer an increased cross-sectional area towards impacting species from the plasma and hence are more susceptible to such etching processes. Thirdly, the longer treatment and therefore longer etching time also results in an increased number of dangling bonds which may partially rearrange into such groups due to the hydrogen deficiency of the Ar/O_2-plasma process.

3.4. *Influence of the process gas*

In order to increase the yield of derivatizable groups, especially alcohol groups, experiments were performed using a wet stream of argon as process gas. Results at 970 μbar and a treatment time of 5 min showed distinctly higher contents in alcohol and carboxyl groups compared to the analogous treatment in an Ar/O_2-plasma, improving from $\Delta[OH]_{Ar/O_2} = 0.18$ groups/100 C-atoms and $\Delta[COOH]_{Ar/O_2} = 0.79$ groups/100 C-atoms to $\Delta[OH]_{Ar-H_2O} = 0.34$ groups/100 C-atoms and $\Delta[COOH]_{Ar-H_2O} = 1.12$ groups/100 C-atoms (see Table 3). We assign this to the increased content of hydrogen in the plasma process and the possibility of respective fractionation products in the plasma such as OH^*, H^*, and O^*. Since the oxidative potential of an OH-radical (OH^*) is even larger than that of atomic oxygen (O^*) and ozone (O_3) [57], this species is the one with the highest probability to react with the substrate and with that the one to contribute the most to the measured effects.

Since lower pressures increased the contents of derivatizable groups in the Ar/O_2-treatments, a pressure variation was

Table 3 – Elemental composition of bucky paper samples treated in an $Ar–H_2O$-plasma at 20 W. Total contents were derived from the plasma-treated samples, fluorine contents were obtained separately for the agent indicated as index. Calculated contents of derivatizable functional groups shown as differences with respect to an untreated sample.

$Ar–H_2O$–20 W	Elemental composition (atom%)					Induced functional groups (per 100 C)		
	C_{total}	O_{total}	F_{TFAA}	F_{TFMPH}	F_{TFE}	Δ[OH]	Δ[C=O]	Δ[COOH]
120 μbar to 5 min	84.9	13.6	5.2	6.1	3.4	1.91	2.25	1.16
260 μbar to 5 min	85.5	13.2	2.7	5.6	3.4	0.82	1.88	1.22
615 μbar to 5 min	85.5	13.5	1.7	5.3	3.1	0.37	1.72	1.06
970 μbar to 5 min	86.0	12.9	1.6	4.8	3.2	0.34	1.47	1.12

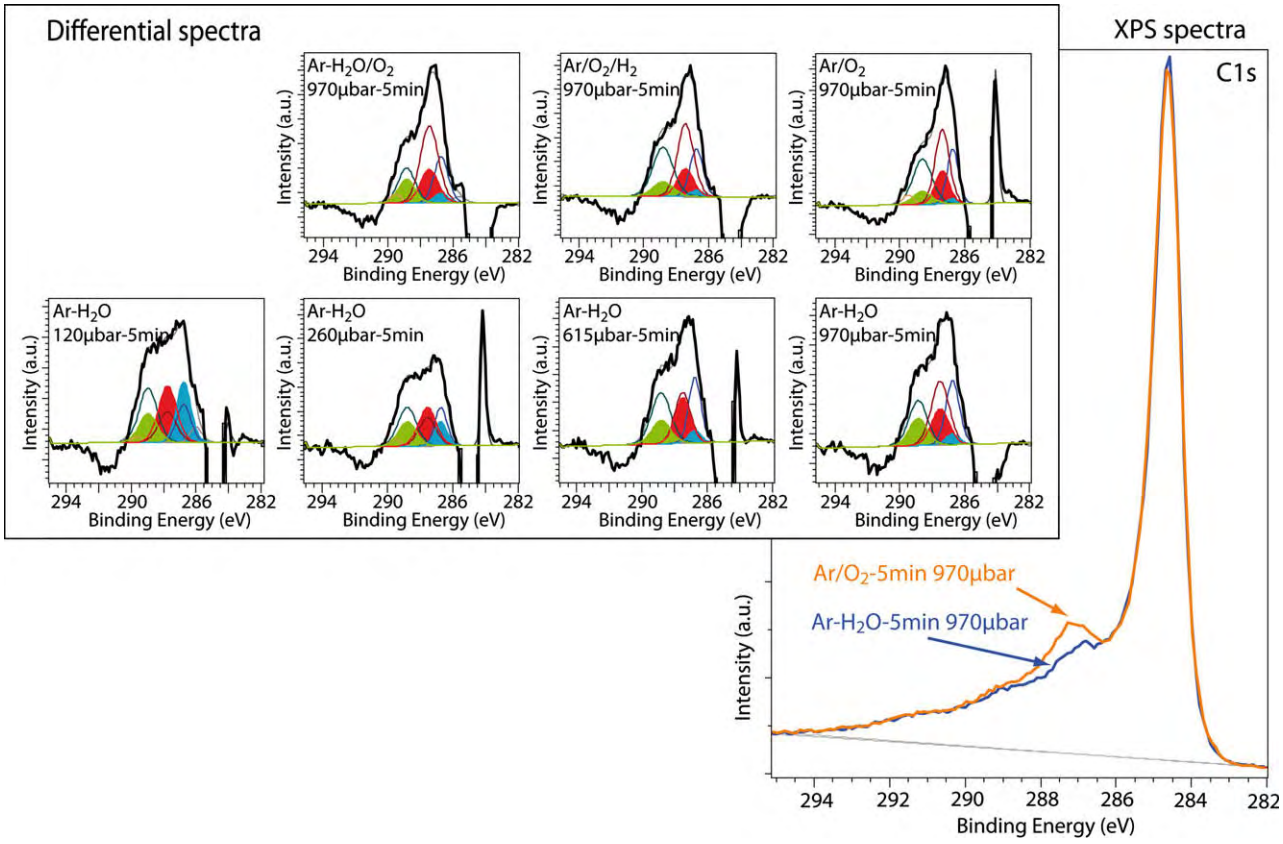

Fig. 4 – XPS spectra recorded on samples treated at 20 W and 970 μbar using an Ar/O_2 or $Ar–H_2O$-plasma (right). Inset (left) shows the C1s differential spectra of samples treated using different gas mixtures and pressures.

carried out using Ar–H_2O-plasmas at 615, 260, and 120 μbar. The contents of keto-/aldehyde-groups and alcohol groups increased considerably up to values of Δ[C=O] = 2.25 groups/100 C-atoms and Δ[OH] = 1.91 groups/100 C-atoms for the treatment at the lowest applied pressure (see Table 3), possibly due to the higher energy per particle. The results obtained from Ar/O_2-treatments were therewith outperformed at least 1.5- and 6-fold, respectively.

Remarkably, the carbon detail spectra (C1s) of the Ar–H_2O-treatments do not show any distinct feature as observed for the Ar/O_2-treatments despite of increased photoelectron intensities in the asymmetric tail (see Fig. 4). Together with the general increase in derivatizable groups, this denotes respectively lower contents of ether-, epoxy, and ester-groups in case of Ar–H_2O. Since the results from the Ar/O_2-treatments have shown that those groups are predominantly generated by ozone, this also implies a significantly reduced ozone content for the Ar–H_2O-plasmas which agrees with findings of Uhlig and Park who independently reported humidity of the process gas to reduce ozone generation [58,59].

Moreover, ESR measurements performed on those samples revealed radical numbers in the range of the untreated reference, indicating effective saturation of plasma induced dangling bonds, most likely due to the increased hydrogen content. This also reduces possible rearrangements in the carbon lattice that may lead or contribute to the formation of ethers and esters as the results for the Ar/O_2-plasmas indicated. In further comparison, Raman spectroscopy held a higher upshift (see Fig. 5) of the D-band for the Ar/O_2-treatment (~3 cm^{-1}) than for the Ar–H_2O-treatment (~2 cm^{-1}). This is to be expected since this technique probes the structural change due to all groups and defects introduced into the CNT lattice. Thus the Raman results agree well with the overall oxygen content and the respectively higher contents in epoxy-, ether-, and ester-groups the derivatization results indicate (in reverse) for the Ar/O_2-treatment. The scattering of the values obtained from Raman analysis is most likely due to the higher resolution of the Raman compared to the XPS, resulting in a respectively higher sensitivity for local differences arising e.g. by morphology reasons.

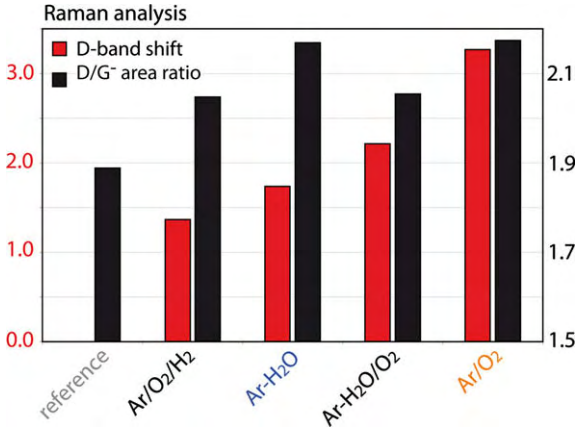

Fig. 5 – Results from Raman analysis of samples treated for 5 min at 970 μbar using different process gas mixtures showing respective D-band shifts and D/G⁻ area ratios with regard to the untreated reference.

Additional experiments at 5 min treatment time and a pressure of 970 μbar were conducted exposing samples to an Ar/O_2/H_2-plasma or an Ar–H_2O/O_2-plasma, respectively. As expected, the addition of hydrogen to the Ar/O_2-mixture decreased the total oxygen content from 14.1 atom% to 13.6 atom% due to the reduced contribution of oxygen to the total process gas flow. In return, addition of oxygen to the Ar–H_2O-mixture led to a slight increase in total oxygen content from 12.9 atom% to 13.1 atom% (see Table 4). Although still being outperformed by the results obtained from the respective Ar–H_2O treatment, the Ar/O_2/H_2-treatment yielded a slight increase in alcohol and carboxyl groups with respect to the respective Ar/O_2-treatment, i.e. from $\Delta[OH]_{Ar/O_2} = 0.18$ groups/100 C-atoms and $\Delta[COOH]_{Ar/O_2} = 0.79$ groups/100 C-atoms to $\Delta[OH]_{Ar/O_2/H_2} = 0.23$ groups/100 C-atoms and $\Delta[COOH]_{Ar/O_2/H_2} = 0.84$ groups/100 C-atoms, acco- mpanied by an ESR signal comparable to that of an untreated sample indicating enhanced saturation of dangling bonds. Yet, the possible generation of OH-radicals may also contribute to this effect.

On the other hand, addition of oxygen to the Ar–H_2O-mixture resulted in slightly enhanced contents of alcohol- and keto-/aldehyde-groups, i.e. from $\Delta[OH]_{Ar-H_2O} = 0.34$ groups/100 C-atoms and $\Delta[C{=}O]_{Ar-H_2O} = 1.47$ groups/100 C-atoms to $\Delta[OH]_{Ar-H_2O/O_2} = 0.37$ groups/100 C-atoms and $\Delta[C{=}O]_{Ar-H_2O/O_2} = 1.65$ groups/100 C-atoms, whereas the amount of carboxyl groups decreased slightly from $\Delta[COOH]_{Ar-H_2O} = 1.12$ groups/100 C-atoms to $\Delta[CO\text{-}\mathit{OH}]_{Ar-H_2O/O_2} = 1.10$ groups/100 C-atoms (see Table 4). This is possibly due to intensified etching caused by the additional oxygen and the larger cross section area of the carboxyl group, paired with their lower stability compared to ester groups. An improved ozone generation is rather improbable since the contribution of the additional oxygen to the total flow was rather small,

Table 4 – Elemental composition of bucky paper samples treated in an Ar/O_2/H_2- and an Ar–H_2O/O_2-plasma at 20 W. Total contents were derived from the plasma-treated samples, fluorine contents were obtained separately for the agent indicated as index. Calculated contents of derivatizable functional groups shown as differences with respect to an untreated sample.

970 μbar to 5 min	Elemental composition (atom%)					Induced functional groups (per 100 C)		
	C_{total}	O_{total}	F_{TFAA}	F_{TFMPH}	F_{TFE}	Δ[OH]	Δ[C=O]	Δ[COOH]
Ar/O_2/H_2	85.4	13.6	1.3	4.5	2.5	0.23	1.28	0.84
Ar–H_2O/O_2	85.9	13.1	1.7	5.2	3.1	0.37	1.65	1.10

i.e. the humidity of the process gas was maintained at an almost constant level.

Evaluation of the D/G^--ratio assessed by Raman, revealed differences for the process gases mentioned (see Fig. 5), yet additional measurements need to be performed for proper interpretation which will be subject to a further publication.[1]

3.5. *Error discussion*

It has to be noted that the fluorine content is influenced by some (systematic) errors that limit the values. First of all, the XPS analysis captures a volume characterized by the spot size on the sample surface and the information depth. Since it has to be assumed that only few layers of the concentric tubes of a MWCNT will be plasma-modified, several layers of pure carbon will be comprised as well, lowering the percentage of fluorine with regard to all detected elements to an average value [15,16]. Second of all, under certain circumstances, the X-ray radiation of the analysis method itself can lead to the destruction of C–F bonds and in turn to a certain loss of intensity. This can be minimized by reducing the power to the X-ray gun and the acquisition time of the spectra. Third of all, a major influence is to be expected from the conversion of the chemical reaction. Data obtained from polymeric substrates [39] does not necessarily need to be applicable to CNT substrates and, to our knowledge, no such data is available for TFMPH. Fourth of all, the general accessibility of the functional groups by the derivatization agents may be affected by sterical hindrance and/or the morphology of the porous bucky papers [60]. Despite of that, the functional groups accessible to the derivatization reagent should also be available for other chemical reactants making the ascertained contents valuable information for further utilization of those groups.

4. Conclusions

Varying process pressure, treatment time and process gas (mixture) we were able to induce different compositions of oxygen functionalities on bucky papers made from MWCNT material. Successful derivatization of plasma-induced functional groups on the surface of CNT sheets could be shown using TFAA for alcohol groups, TFMPH for keto-/aldehyde groups, and TFE for carboxyl groups.

With decreasing pressure, both Ar/O_2 and $Ar–H_2O$ treatment showed increasing contents of alcohol and keto-/aldehyde groups. For the Ar/O_2 treatments the higher pressure treatments were accompanied by increasing radical numbers, i.e. dangling bonds, and a lower intensity of emitting species of atomic oxygen. Despite of almost identical total oxygen contents, the treatments at higher pressure held lower contents in alcohol groups and especially for longer treatment times also lower contents in carboxyl groups. Yet, XPS spectra showed an increased intensity around 287 eV and almost identical intensities for binding energies >288 eV for those treatments. This was assigned to an increasing ozone content most likely to elicit epoxy- and ester-groups as well as an enhanced etching resulting in the larger number of dangling bonds.

Medium treatment times (5 min) yielded comparatively high oxygen contents as well as improved contents of keto-/aldehyde and carboxyl groups with respect to corresponding treatments at 10 min, signifying a shorter influence time of plasma-generated ozone and the etching effect caused by both, atomic oxygen and ozone. With increasing hydrogen concentration in the process gas, contents of derivatizable groups increased, while radical numbers diminished to values close to the untreated reference. This was assigned to an effective saturation of plasma induced dangling bonds and an entailed prevention of possible rearrangements in the carbon lattice. Addition of oxygen to an $Ar–H_2O$-plasma indicated potential towards higher contents in alcohol and keto-/aldehyde groups, yet at the expense of an increased etching potential and an arising effect especially on less stable functional groups of larger cross section areas such as carboxyl groups.

The highest contents in derivatizable functional groups which outperformed all others up to 6-fold, were measured for treatments in $Ar–H_2O$-plasmas at the lowest pressure applied. Here, the highly oxidizing OH-radical combined with a high energy per particle and an effective saturation of dangling bonds by sufficient presence of hydrogen meet a significantly reduced or even inhibited generation of ozone due to the humidity of the process gas mixture.

The results described in this contribution, the application of derivatization procedures, and the use of the so-gained data for the generation of differential XPS-spectra constitute a valuable step towards a better understanding of the effects of plasma treatments on CNT substrates. We have thereby demonstrated a way to assess the contents of different functional groups accessible to a subsequent wet chemical processing. In consideration of the effects limiting the amount of derivatizable functional groups and measurable fluorine content and assuming similar chemical conversions with other substances, the contents evaluated herein constitute the minimal values utilizable for further applications. The transfer of this experience to the modification of the powdery CNT raw material will be subject to a further publication.[2]

Acknowledgements

The authors thank Mr. Bjoern Moller for producing the bucky papers and Mr. Georg Kammer for helping conducting the ESR measurements. Parts of this work were funded by the German Federal Ministry of Education and Research Project PLASMITT (No. 13N9004) and by the Fraunhofer Gesellschaft zur Förderung der Angewandten Forschung e.V.

[1] Katzenmaier V, Zschoerper NP, Haupt M, Vohrer U, Oehr C. New insights in raman spectroscopy of carbon nanotube sheets. To be published.

[2] Zschoerper NP, Vohrer U, Oehr C. Plasmamodification of carbon nanotube powders in fluidized bed reactors of different geometries. To be published.

REFERENCES

[1] Radushkevich LV, Lukyanovich VM. O strukture ugleroda, obrazujucegosja pri termiceskom razlozenii okisi ugleroda na zeleznom kontakte. Russ J Phys Chem 1952;26:88–95.
[2] Iijima S. Helical microtubulus of graphitic carbon. Nature 1991;354:56–8.
[3] Iijima S, Ichihashi T. Single-shell carbon nanotubes of 1-nm diameter. Nature 1993;363:603–5.
[4] Bethune DS, Kinag CH, Devrics MS, Gorman G, Savoy R, Vascuez J, et al. Cobalt-catalysed growth of carbon nanotubes with single-atomic-layer walls. Nature 1993;363:605–7.
[5] Ajayan PM. Nanotubes from carbon. Chem Rev 1999;99(7):1787–800.
[6] Dai H. Carbon nanotubes: opportunities and challanges. Surf Sci 2002;500(1–3):218–41.
[7] Meyyappan M, editor. Carbon nanotubes – science and applications. CRC Press; 2005. p. 137–279.
[8] Fang HT, Liu CG, Liu C, Li F, Liu M, Cheng HM. Purification of single-wall carbon nanotubes by electrochemical oxidation. Chem Mater 2004;16(26):5744–50.
[9] Hirsch A, Vostrowsky O. Functionalization of carbon nanotubes. Funct Mol Nanostruct 2005:193–237.
[10] Kim B, Sigmund WM. Functionalized multiwall carbon nanotube/gold nanoparticle composites. Langmuir 2004;20(19):8239–42.
[11] Sumanasekera GU, Allen JL, Fang SL, Loper AL, Rao AM, Eklund PC. Electrochemical oxidation of single wall carbon nanotube bundles in sulfuric acid. J Phys Chem B 1999;103(21):4292–7.
[12] Morita S, Hattori S. Applications of plasma polymers. In: d' Agostino R, editor. Plasma deposition, treatment, and etching of polymers. Boston: Academic Press, Inc.; 1990. p. 423–61.
[13] Yasuda H. Plasma polymerization. London: Academic Press; 1985. p. 344–54.
[14] d'Agostino R, Favia P, Oehr C, Wertheimer MR. Low-temperature plasma processing of materials: past, present, and future. Plasma Process Polym 2005;2:7–15.
[15] Vohrer U, Zschoerper NP, Koehne Y, Langowski S, Oehr C. Plasma modification of carbon nanotubes and bucky papers. Plasma Process Polym 2007;4:S871–7.
[16] Bubert H, Haiber S, Brandl W, Marginean G, Heintze M, Brüser V. Characterization of the uppermost layer of plasma-treated carbon nanotubes. Diam Relat Mater 2003;12:811–5.
[17] Zschoerper NP, Vohrer U, Oehr C, Brunner H. Plasmabehandlung von Carbon Nanotube Pulver und Bucky Papers. 13 Fachtagung Plasmatechnologie (PT 13), 06 March 2007, Bochum; 2007. p. 65–6.
[18] Tseng C-H, Wang C-C, Chen C-Y. Modification of multi-walled carbon nanotubes by plasma treatment and further use as templates for growth of CdS nanocrystals. Nanotechnology 2006;17(22):5602–12.
[19] Vohrer U, Zschoerper NP, Katzenmaier V. Carbon nanotubes – materials for the 21st century? NanoS 2007;3:9–13.
[20] Tseng CH, Wang CC, Chen CY. Functionalizing carbon nanotubes by plasma modification for the preparation of covalent-integrated epoxy composites. Chem Mater 2007;19(2):308–15.
[21] Yan YH, Chan-Park MB, Zhou Q, Li CM, Yue CY. Functionalization of carbon nanotubes by argon plasma-assisted ultraviolet grafting. Appl Phys Lett 2005;87(21):213101-1–3.
[22] Yan YH, Cui J, Chan-Park MB, Wang X, Wu QY. Systematic studies of covalent functionalization of carbon nanotubes via argon plasma-assisted UV grafting. Nanotechnology 2007;18:1–7.
[23] Felten A, Bittencourt C, Pireaux JJ, Van Lier G, Charlier JC. Radio-frequency plasma functionalization of carbon nanotubes surface O_2, NH_3, and CF_4 treatments. J Appl Phys 2005;98(7):074308-1–9.
[24] Khare B, Wilhite P, Tran B, Teixeira E, Fresquez K, Mvondo DN, et al. Functionalization of carbon nanotubes via nitrogen glow discharge. J Phys Chem B 2005;109(49):23466–72.
[25] Khare BN, Wilhite P, Quinn RC, Chen B, Schingler RH, Tran B, et al. Functionalization of carbon nanotubes by ammonia glow-discharge: experiments and modeling. J Phys Chem B 2004;108(24):8166–72.
[26] Ruelle B, Felten A, Ghijsen J, Drube W, Johnson RL, Liang D, et al. Functionalization of MWCNTs with atomic nitrogen: electronic structure. J Phys D: Appl Phys 2008;41(4):045202-1–4.
[27] Chirila V, Marginean G, Brandl W. Effect of the oxygen plasma treatment parameters on the carbon nanotubes surface properties. Surf Coat Technol 2005;200(1–4):548–51.
[28] Vohrer U, Zschoerper NP, Moller BP. Carbon nanotubes – a material rising like a phoenix. Vakuum in Forschung und Praxis – Vacuums Best 2008;20(S1):38–46.
[29] Felten A, Bittencourt C, Colomer JF, Van Tendeloo G, Pireaux JJ. Nucleation of metal clusters on plasma treated multi wall carbon nanotubes. Carbon 2007;45(1):110–6.
[30] Felten A, Bittencourt C, Pireaux JJ. Gold clusters on oxygen plasma functionalized carbon nanotubes: XPS and TEM studies. Nanotechnology 2006;17:1954–9.
[31] Majumder M, Chopra N, Hinds BJ. Effect of tip functionalization on transport through vertically oriented carbon nanotube membranes. J Am Chem Soc 2005;127(25):9062–70.
[32] Imasaka K, Suehiro J, Kanatake Y, Kato Y, Hara M. Preparation of water-soluble carbon nanotubes using a pulsed streamer discharge in water. Nanotechnology 2006;14:3421–7.
[33] Imasaka K, Kato Y, Suehiro J. Enhancement of microplasma-based water-solubilization of single-walled carbon nanotubes using gas bubbling in water. Nanotechnology 2007;18:335602-1–7.
[34] Huang S, Dai L. Plasma etching for purification and controlled opening of aligned carbon nanotubes. J Phys Chem B 2002;106(14):3543–5.
[35] Chopra N, Majumder M, Hinds BJ. Bifunctional carbon nanotubes by sidewall protection. Adv Funct Mater 2005;15(5):858–64.
[36] Xu T, Yang J, Liu J, Fu Q. Surface modification of multi-walled carbon nanotubes by O_2 plasma. Appl Surf Sci 2007;253(22):8945–51.
[37] Xia W, Schluter OFK, Liang C, van den Berg MWE, Guraya M, Muhler M. The synthesis of structured Pd/C hydrogenation catalysts by the chemical vapor deposition of Pd(allyl)Cp onto functionalized carbon nanotubes anchored to vapor grown carbon microfibers. Catal Today 2005;102–103:34–9.
[38] Rinzler AG, Liu J, Dai H, Nikolaev P, Huffman CB, Rodriguez-Macias FJ, et al. Large-scale purification of single-wall carbon nanotubes: process, product, and characterization. Appl Phys A 1998(67):29–37.
[39] Sabbatini L, Zambonin PG, editors. Surface characterization of advanced polymers. Weinheim; New York; Basel; Cambridge; Tokyo: VCH; 1993. p. 221–56.
[40] Dickie RA, Hammond JS, De Vries JE, Holubka JW. Surface derivatization of hydroxyl functional acrylic copolymers for characterization by X-ray photoelectron spectroscopy. Anal Chem 1982;54(12):2045–9.
[41] Briggs D, Kendall CR. Derivatization of discharge-treated LDPE: an extension of XPS analysis and a probe of specific interactions in adhesion. Int J Adhes Adhes 1982;2(1):13–7.
[42] Briggs D. XPS studies of polymer surface modifications and adhesion mechanisms. J Adhesion 1982;13(3):287–301.

[43] Gerenser LJ, Elman JF, Mason MG, Pochan JM. E.s.c.a. studies of corona-discharge-treated polyethylene surfaces by use of gas-phase derivatization. Polymer 1985;26(8):1162–6.
[44] Vohrer U, Hegemann D, Oehr C. XPS, AES, and AFM as tools for study of optimized plasma functionalization. Anal Bioanal Chem 2003;375(7):929–34.
[45] Vohrer U, Blomfield C, Page S, Roberts A. Quantitative XPS imaging-new possibilities with the delay-line detector. Appl Surf Sci 2005;252(1):61–5.
[46] Wang YQ, Sherwood PMA. Studies of carbon nanotubes and fluorinated nanotubes by X-ray and ultraviolet photoelectron spectroscopy. Chem Mater 2004;16(25):5427–36.
[47] Horowitz A, von Helden G, Schneider W, Simon FG, Crutzen PJ, Moortgat GK. Ozone generation in the 214-nm photolysis of oxygen at 25 °C. J Phys Chem 1988;92(17):4956–60.
[48] Devins JC. Mechanism of ozone formation in the silent electric discharge. J Electrochem Soc 1956;103(8):460–6.
[49] Pignolet P, Hadj-Ziane S, Held B, Peyrous R, Benas JM, Coste C. Ozone generation by point to plane corona discharge. J Phys D: Appl Phys 1990;23(8):1069–72.
[50] Lu X, Zhang L, Xu X, Wang N, Zhang Q. Can the sidewalls of single-wall carbon nanotubes be ozonized? J Phys Chem B 2002;106:2136–9.
[51] Lu X, Chen Z, Schleyer PvR. Are Stone–Wales defect sites always more reactive than perfect sites in the sidewalls of single-wall carbon nanotubes? J Am Chem Soc 2005;127:20–1.
[52] Mawhinney DB, Naumenko V, Kuznetsova A, Yates JT, Liu J, Smalley RE. Infrared spectral evidence for the etching of carbon nanotubes: ozone oxidation at 298 K. J Am Chem Soc 2000;122(10):2383–4.
[53] Yim WL, Liu ZF. A reexamination of the chemisorption and desorption of ozone on the exterior of a (5,5) single-walled carbon nanotube. Chem Phys Lett 2004;398(4–6):297–303.
[54] Byl O, Liu J, Yates JT. Etching of carbon nanotubes by ozones – a surface area study. Langmuir 2005;21:4200–4.
[55] Criegee R. Mechanism of ozonolysis. Angew Chem Int Ed Engl 1975;14(11):745–52.
[56] Heymann D, Bachilo SM, Weisman RB, Cataldo F, Fokkens RH, Nibbering NMM, et al. C60O3, a fullerene ozonide: synthesis and dissociation to C60O and O_2. J Am Chem Soc 2000;122:11473–9.
[57] Chen Q, Fu Y-B, Zhang C-M, Zhang Y-F, Yang L-Z. The role of hydroxyl and atomic oxygen in multiwall carbon nanotube growth. Front Mater Sci China 2008;2(1):20–5.
[58] Uhlig P, Haacke M, Pietsch GJ. On the impact of the feed gas quality on the efficiency of ozone generation. In: 14th Ozone world congress, August 22–28 1999, Dearborn, Michigan, USA; 1999. p. 150–3.
[59] Park JS, Kim KH, Kwon GJ, Lukanin A, Khasanov O, Kim YS, et al. Development of small and efficient ozone generators using coronadischarge. In: KORUS '01 proceedings the fifth Russian-Korean international symposium on science and technology, 2001, vol. 1; 2001. p. 282–4.
[60] Unger WES. Surface chemical analysis of plasma polymer films: how far shines the light today? Vakuum in Forschung und Praxis 2008;20(4):20–7.